SLAC–PUB–5143
November 1989
(E/T)

MEASUREMENT OF THE Z BOSON RESONANCE PARAMETERS*

G. J. FELDMAN
Stanford Linear Accelerator Center,
Stanford University, Stanford, CA 94309

ABSTRACT

Using the Mark II detector at the SLC, we measure the Z mass and width to be 91.17 $\pm$ 0.18 GeV/c^2 and $1.95^{+0.40}_{-0.30}$ GeV, respectively. From a fit in which the visible Z width is constrained to its Standard Model value, the number of neutrino species is determined to be 3.0 ± 0.9 or < 4.4 at the 95% confidence level.

INTRODUCTION

There will be two presentations from the Mark II Collaboration[1] today. The division of labor is rather simple. I will talk about the production of Z bosons and Professor Weinstein will talk about their decay.

Three weeks ago, we submitted our initial measurements of the Z resonance parameters for publication in *Physical Review Letters*.[2] The results were

$$m = 91.11 \pm 0.23 \text{ GeV/c}^2 , \quad (1)$$

$$\Gamma = 1.61^{+0.60}_{-0.43} \text{ GeV} , \text{ and} \quad (2)$$

$$N_\nu = 3.8 \pm 1.4 . \quad (3)$$

Today, we will update these measurements based on two major improvements:

1. a doubling of the data from 106 events to 233 events, and
2. the use of the MiniSAM for point-to-point normalization.

This will result in a substantial improvement in the precision of these measurements.

We want to determine the Z boson resonance parameters by comparing the rate of Z formation in e^+e^- annihilation (Fig. 1) as a function of the center-of-mass energy, E, with that for a process with a known cross section, Bhabha (e^+e^-) scattering (Fig. 2). To accomplish this, we have to do four things:

1. measure E,

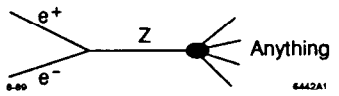

Figure 1: Z formation in e^+e^- annihilation.

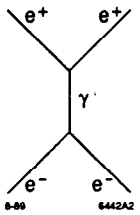

Figure 2. Small-angle Bhabha scattering.

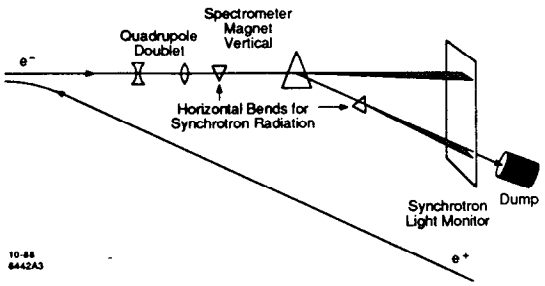

Figure 3. Schematic of one of the energy spectrometers.

2. count Z's,
3. count Bhabha scatters, and
4. fit the ratios to obtain the Z parameters.

The above list will serve as an outline for this talk. I will simply explain how we do each of these things.

* Work supported by Department of Energy contract DE–AC03–76SF00515.

Invited talk presented at the XIV International Symposium on Lepton and Photon Interactions, Stanford, California, August 7–12, 1989.

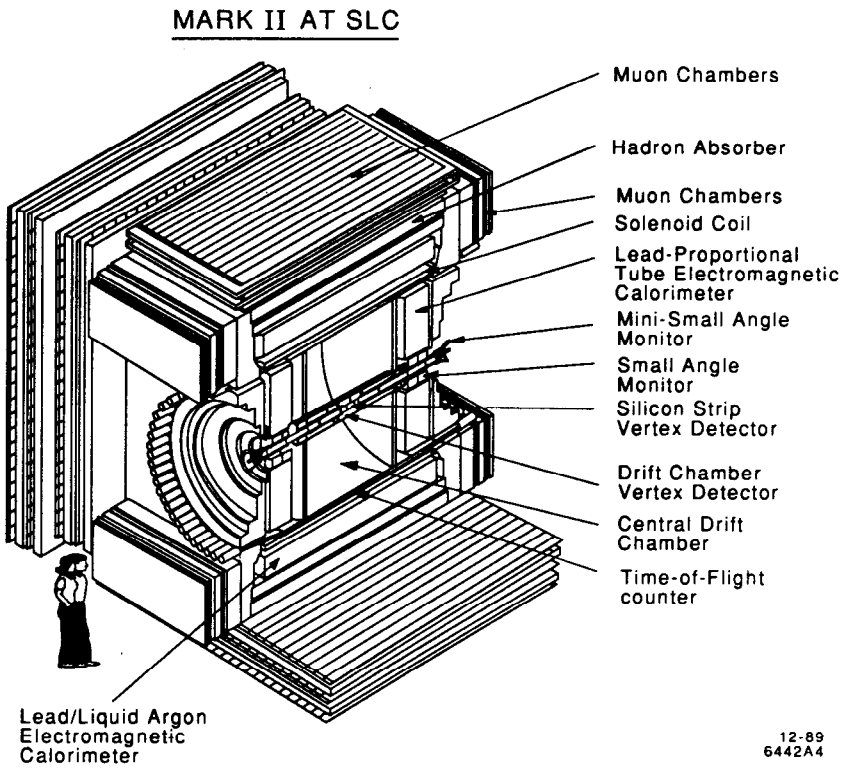

Figure 4. The Mark II detector.

Absolute Energy Measurement

We have built spectrometers of a novel design to measure the absolute energies of both beams to high accuracy.[3] Figure 3 shows a schematic drawing of one of the spectrometers. The electron beam first passes through a horizontal bend and emits a horizontal swath of synchrotron radiation in the initial electron beam direction. It then passes through an accurately-measured spectrometer magnet which bends it down. Finally, it traverses a second horizontal bend to give another swath of synchrotron radiation in the direction of the outgoing beam. The two swaths of synchrotron radiation are intercepted by a phosphorescent screen. It is clear that the mean energy of beam can be measured from the knowledge of three quantities:

1. the magnetic-field integral of the spectrometer magnet,
2. the distance between the center of the spectrometer magnet and the screen, and
3. the distance between the two synchrotron radiation swaths on the screen.

The spectrometer magnet field integral has been calibrated to a few parts in 10^5 by two independent techniques and is constantly measured by a rotating coil. The distance between the magnet center and the screen is determined to high precision by surveying techniques, and the distances on the screen are calibrated by accurately placed fiducial wires.

The systematic uncertainties in the measurement of each beam (itemized in Table 1) total to 20 MeV. Allowing for a possible correlation between beam dispersion and offset, the total systematic uncertainly in the measurement of E is 40 MeV.

Table 1: Systematic uncertainties in the energy measurement of each beam.

Item	Uncertainty (MeV)
Magnetic measurement	5
Detector resolution	10
Magnet rotation	16
Survey	5
Total	20

Table 2: Mark II triggers.

Purpose	Trigger	Requirements
Z decays	Charged	$\geq$ 2 charged tracks with $p_t > 150$ MeV/c and $\|\cos\theta\| < 0.75$.
	Neutral	A single deposition of $\geq$ 2.2 GeV in the endcap calorimeter or $\geq$ 3.3 GeV in the barrel calorimeter.
Luminosity	SAM	$\geq$ 6 GeV in both detectors.
	MiniSAM	$\geq$ 15 GeV in both detectors.
Diagnostic	Random	Random beam crossings.
	Cosmic	Taken between beam crossings.

The energy spread of each beam is also measured to about 30% accuracy by the increased dispersion caused by the spectrometer magnet. The mean energy and energy spread are measured on every SLC pulse and are read by the Mark II on every trigger.

MARK II DETECTOR

A drawing of the Mark II detector[4] is shown in Fig. 4. The principal components which we will be interested in today will be the drift chamber, the calorimeters, and the luminosity monitors.

The drift chamber is a 72-layer, mini-jet cell, cylindrical chamber[5] immersed in 4.75 kG solenoidal magnetic field. It tracks charged particles in the region $|\cos\theta| < 0.92$, but the efficiency and momentum resolution begin to deteriorate at $|\cos\theta| = 0.82$. Without a vertex constraint, the momentum resolution is about $0.5\%p$ (p in GeV/c).

There are two sets of electromagnetic calorimeters, which, together, detect photons in the region $|\cos\theta| < 0.96$. The central calorimeters are lead-liquid argon sandwich ionization chambers[6] with an energy resolution of about $14\%/\sqrt{E}$ (E in GeV). The forward and backward calorimeters are composed of lead-gas proportional tube sandwiches with energy resolution of about $22\%/\sqrt{E}$. Both calorimeters have a strip geometry with three or four strip directions for stereographic reconstruction.

Figure 5 shows a close-up of the region around the beam-line. Note the two luminosity monitors at small angles, the Small Angle Monitor (SAM), followed at smaller angles by the MiniSAM.

TRIGGERS

The six main Mark II triggers are listed in Table 2. Monte Carlo simulations indicate that the charged and neutral triggers are 97% and 95% efficient for Z hadronic decays, respectively. In addition to being highly redundant, they are complementary in that the charged trigger is more efficient in the central region, while the neutral trigger is more efficient in the forward and backward regions. Together, they are calculated to be 99.8% efficient. (This number is irrelevant because, as we will see shortly, we will not be able to identify all of these decays.) Of the 215 hadronic events used in the present analysis, 211 satisfied both the charged and neutral trigger.

The random trigger is used to correct for beam-induced backgrounds. For example, in all Mark II SLC analyses, randomly triggered events are combined with Monte Carlo simulations of physical processes to give a complete simulation of both the physics and the backgrounds. In the next section we will see an important application of this technique.

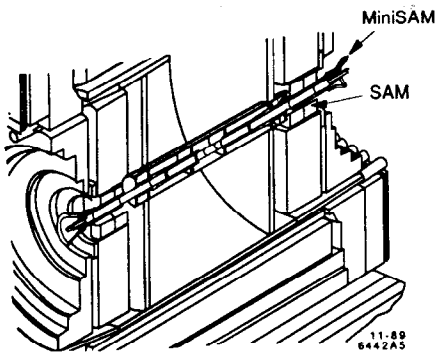

Figure 5. Detail around the beam line of the Mark II detector.

LUMINOSITY MEASUREMENTS

To obtain the optimum absolute and relative luminosity measurements we use a well-defined fiducial region of the SAM to measure the absolute luminosity, while we use the total SAM and the MiniSAM to determine the relative, or point-to-point, luminosity. The geometrical acceptance of these detectors is illustrated in Fig. 6.

Absolute Luminosity Measurement

A drawing of the SAM is shown in Fig. 7. Each SAM consists of nine layers of drift tubes for tracking and a six-layer lead-proportional-tube sandwich

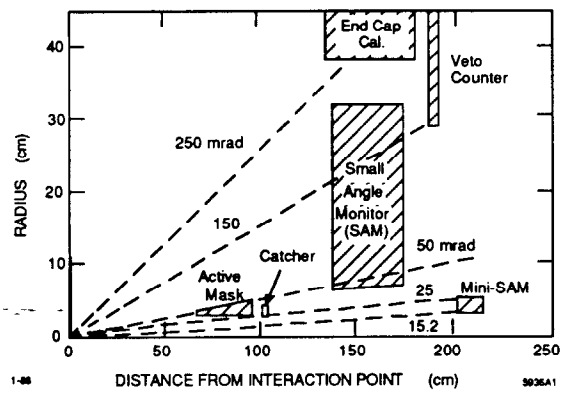

Figure 6. Geometrical acceptances of the SAM and MiniSAM.

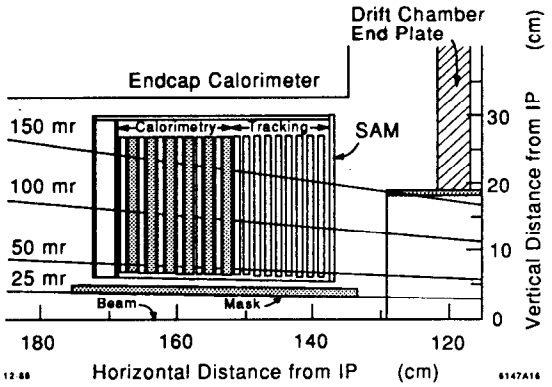

Figure 7. The Small Angle Monitor (SAM).

for measuring the electron energy and position. A typical event is shown in Fig. 8. The tracking information is not always available due to backgrounds, but the calorimetric reconstruction of the electron pulse is unmistakable and background free. The angular resolution from the shower reconstruction is about a milliradian.

Figures 9 and 10 show some of the results from the reconstructed shower measurements in the SAMs. Figure 9 shows the acollinearity angle compared with Monte Carlo calculations. Figure 10 shows the distribution in θ, the angle between the incident and scattered electron versus the number of events divided by θ^3. This quantity should be a horizontal line for full acceptance. The effect of the acceptance-defining mask can be clearly seen, and the region used for the precise luminosity measurement is shown.

The technique for determining the absolute luminosity was to count events with both the electron

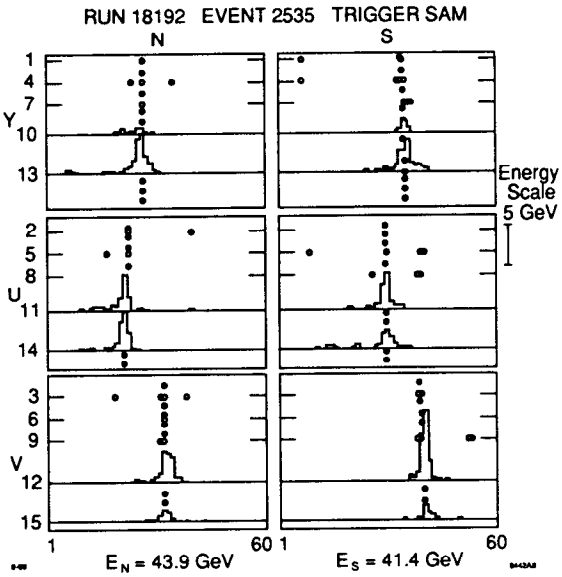

Figure 8. A typical SAM event.

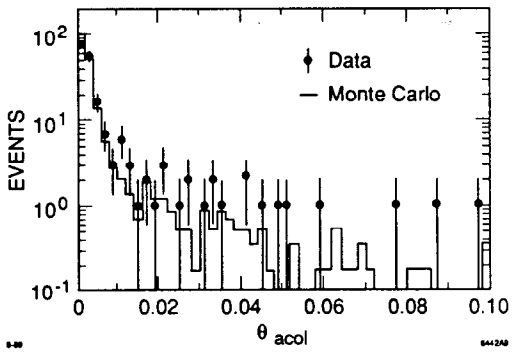

Figure 9. Acollinearity angle for Bhabha scattering events in the SAMs.

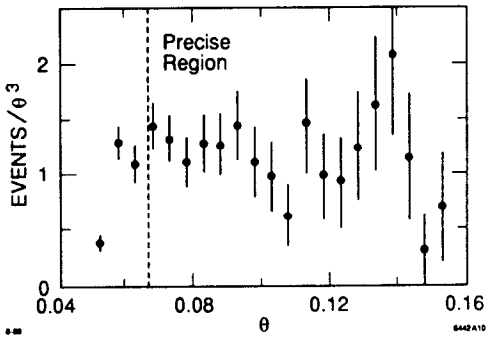

Figure 10. Angular distribution of Bhabha scattering events in the SAMs divided by θ^3.

and positron tracks in the angular region $65 < \theta < 160$ mrad with unit weight and events with only one track in this with region with half weight. This is a standard technique to reduce the sensitivity of the measurement to possible misalignments and detector resolution.

There were 236 events with both tracks and 21 events with only one track in the precise region. The cross section corresponding to the precise region was calculated to be 24.9 nb at 91 GeV.[7]

The systematic uncertainties in the absolute luminosity measurement total 3.0% and are equally divided between unknown higher-order radiative corrections and the effect of detector resolution on the SAM precise region acceptance.

Relative Luminosity Measurement

The most important part of the point-to-point luminosity measurement are the MiniSAMs, a drawing of which is shown in Fig. 11. These are simple tungsten-scintillator sandwiches divided into four quadrants which are separately read out.

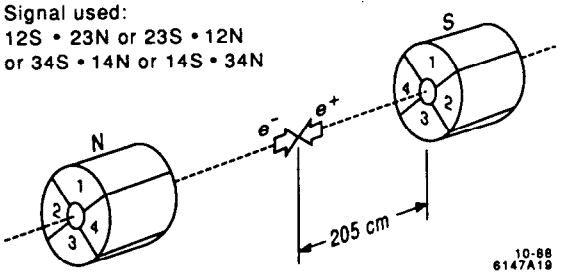

Figure 11. The MiniSAMs.

The requirement for detecting a Bhabha scattering event in the MiniSAMs is

1. back-to-back quadrants each with more than 15 GeV,
2. no nonadjacent quadrant with more than 15 GeV, and
3. time-of-flight measurement in all quadrants with more than 15 GeV consistent with Bhabha scattering.

There are two major sources of systematic error associated with the MiniSAMs. First the beam positions and angles can change from point to point. We track these changes closely and have concluded that they lead to a negligible error.

The second source is potentially more serious. Beam-related backgrounds can prevent the

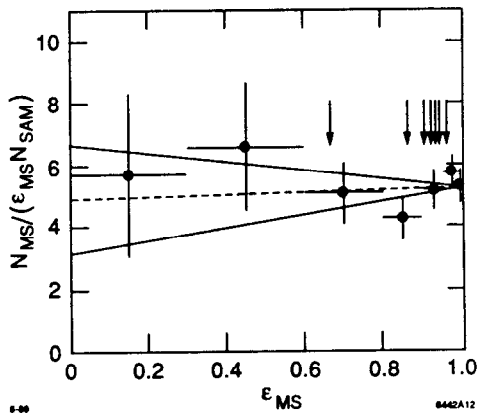

Figure 12. The ratio of the efficiency-corrected MiniSAM rate to the SAM rate as a function of the MiniSAM efficiency. The dashed line indicates a best fit, and the solid lines indicate the 1σ limits on the fit. The efficiencies of the seven scan points are shown by arrows.

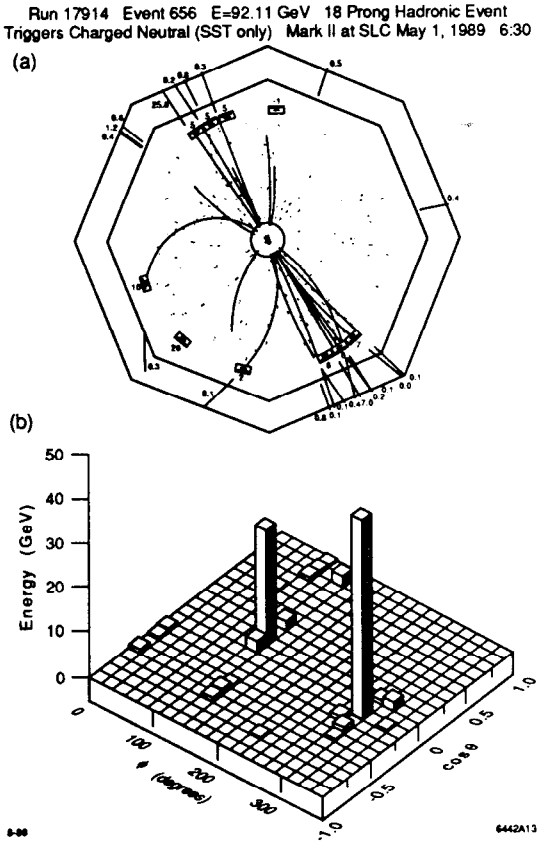

Figure 13. (a) A computer reconstruction of a typical hadronic Z decay viewed along the beam axis. (b) A plot of the detected energy for this event as a function of the azimuthal angle and the cosine of the polar angle.

MiniSAMs from meeting the above requirements for an otherwise valid Bhabha scattering event. To determine the magnitude of this effect, the raw data from Bhabha scattering events created by Monte Carlo simulations are added to randomly triggered events to determine if the events would have been counted if they had occurred. In this way, a MiniSAM efficiency is calculated for each run. The average efficiency was 90%, but it varied from 65% to 96% on different scan points.

Figure 12 shows the ratio of the efficiency-corrected MiniSAM rate to the SAM rate as a function of the MiniSAM efficiency. There is no indication that the efficiency calculation is biased, but we parameterize the uncertainty in the fit, shown by solid lines, as a possible systematic error.

Z DECAY EVENT SELECTION

Figure 13(a) shows a typical hadronic Z decay. The two-jet structure, shown graphically in the Lego plot of Fig. 13(b), and the charged multiplicity of about 20 tracks are typical of these events. About 7/8 of visible Z decays are into hadronic modes. The remainder are split among e, μ, and τ pairs. A τ pair decay is shown in Fig. 14, in which one of the τs decays into a 16 GeV/c muon and the other decays into a 17 GeV/c electron.

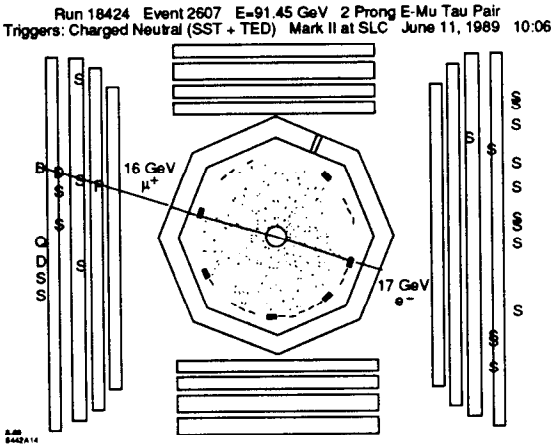

Figure 14. A computer reconstruction of a Z decay into τ pairs.

Z production is the dominant annihilation process, so the selection criteria can be quite loose. The only possible backgrounds come from beam-gas interactions and γ–γ interactions. Both of these process leave a large amount of energy in at most one of the forward-backward hemispheres.

Accordingly, the criteria for hadronic Z decays are:

1. $\geq$ 3 charged tracks from a cylindrical volume around the interaction point with a radius of 1 cm and a half-length of 3 cm, and
2. at least 0.05 E visible in both the forward and backward hemispheres.

These criteria give an efficiency of 94.5 $\pm$ 0.5%.

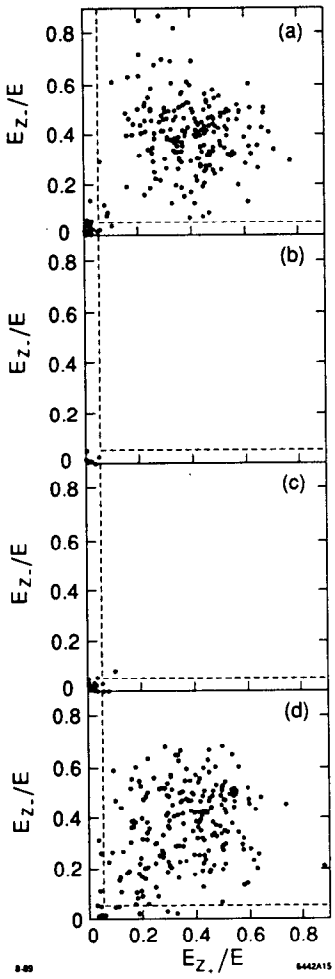

Figure 15. Fractional energies in the forward versus backward hemispheres for events with three or more charged tracks from the fiducial region for (a) events from the region of the interaction point, (b) events displaced along the beam line by $\pm$10 and $\pm$16 cm (four times the fiducial volume), (c) a Monte Carlo simulation of γ–γ interactions with 40 times the integrated luminosity, and (d) a Monte Carlo simulation of Z hadronic decays. The lines indicate the region for acceptable events.

Figure 15 shows the possible level of backgrounds. Each event with 3 or more charged tracks

from the fiducial region is shown on a scatter plot of the amount of energy in each hemisphere expressed as a fraction of E. Figure 15(a) shows the data from the region of the interaction point. There is a diffuse cluster of events which meet the acceptance criteria and a another cluster near zero energy in both hemispheres. Figure 15(b) shows the distribution of beam-gas interactions. It is constructed by taking the fiducial regions displaced along the beam line by ± 10 and ± 16 cm, giving four times the fiducial volume. No event is within the acceptable region.

Figure 15(c) shows the results of a Monte Carlo simulation of γ–γ interactions corresponding to forty times the present luminosity. One event passes the acceptance criteria. Finally, Fig. 15(d) shows the result of a Monte Carlo simulation of Z hadronic decays. These plots demonstrate that the Z hadronic decays are essentially background-free.

To increase our statistical precision slightly, we also accept those leptonic Z decays for which the efficiency is high and the identification and interpretation is clear, namely, μ and τ pairs in the angular region $|\cos\theta| < 0.65$. To avoid backgrounds from γ–γ interactions, we require a minimum of 0.10 E visible energy for τ pairs. The efficiencies for detecting μ and τ pairs within the fiducial angular region are $99 \pm 1\%$ and $96 \pm 1\%$, respectively.

The data are shown in Table 3 and Fig. 16. Note that we plot an unusual quantity, but one that is closely related to what we actually measure, the cross sections for all hadronic decays and $\mu^+\mu^-$ and $\tau^+\tau^-$ with $|\cos\theta| < 0.65$. The rest of this talk discusses how we get information on the Z resonance parameters from these data.

FITS TO THE DATA

We perform maximum-likelihood fits using Poisson statistics to a relativistic Breit–Wigner line shape

$$\sigma(E) = \frac{12\pi}{m^2}\frac{s\Gamma_{ee}(\Gamma - \Gamma_{inv})}{(s-m^2)^2 + s^2\Gamma^2/m^2}[1+\delta(E)] \quad , \quad (4)$$

where Γ is the total width and Γ_{inv} is the partial width into invisible decay modes, *i.e.*, into neutrinos and neutrino-like particles. Large effects due to initial state radiation, represented in Eq. (4) by $[1+\delta(E)]$, are calculated by an analytic form due to Cahn.[9] Alexander *et al.* have shown that this form has more than sufficient accuracy for our purposes.[10]

A Breit–Wigner shape has three parameters, a position, a width, and a height. We can fit for these three parameters as m, Γ, and Γ_{inv}, or equivalently, the number of neutrino species, N_ν.

The mass and width clearly determine the position and width of the resonance. The height is most sensitive to the third parameter, Γ_{inv}. This comes about because a Breit–Wigner is proportional to the partial width to the initial state times the partial width to the final state. The partial width to the initial state, e^+e^-, is well determined in the Standard Model. The final state can be taken to be all of the final states that we can see, in principle, in our detector, *i.e.*, all states except those into neutrino pairs (or pairs of neutrino-like objects).

Another way of viewing this is the following: If we could detect all of the final states, and if we integrated the resonance over energy, then we would find that the integral only depends on the width to the initial state. This is a statement that we pro-

Table 3: Summary of the data. (a) The errors do not include an overall 6.7% normalization uncertainty. (b) The total of 233 events is composed of 215 hadronic decays, 7 $\mu^+\mu^-$, and 11 $\tau^+\tau^-$. (c) Cross sections are for all hadronic decays and $\mu^+\mu^-$ and $\tau^+\tau^-$ with $|\cos\theta| < 0.65$. The errors are for 68.3% confidence level integrals. See Ref. [8].

$< E >$ (GeV)	$\int \mathcal{L}dt^{(a)}$ (nb^{-1})	$N_Z{}^{(b)}$	$\sigma_Z{}^{(a,c)}$ (nb)
89.24	0.67 ± 0.05	3	$4.6^{+4.6}_{-2.5}$
89.98	0.82 ± 0.06	10	$13.1^{+5.8}_{-4.2}$
90.74	1.31 ± 0.07	36	$30.5^{+6.4}_{-5.3}$
91.06	4.25 ± 0.13	120	$31.2^{+3.3}_{-3.0}$
91.50	1.33 ± 0.08	39	$32.4^{+6.5}_{-5.5}$
92.16	0.58 ± 0.05	11	$19.8^{+8.4}_{-6.1}$
92.96	1.10 ± 0.08	14	$13.0^{+4.7}_{-3.6}$
Totals	9.89 ± 0.21	233	

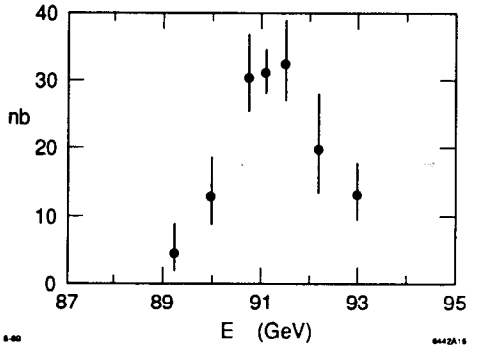

Figure 16. The cross sections for all hadronic decays and $\mu^+\mu^-$ and $\tau^+\tau^-$ with $|\cos\theta| < 0.65$.

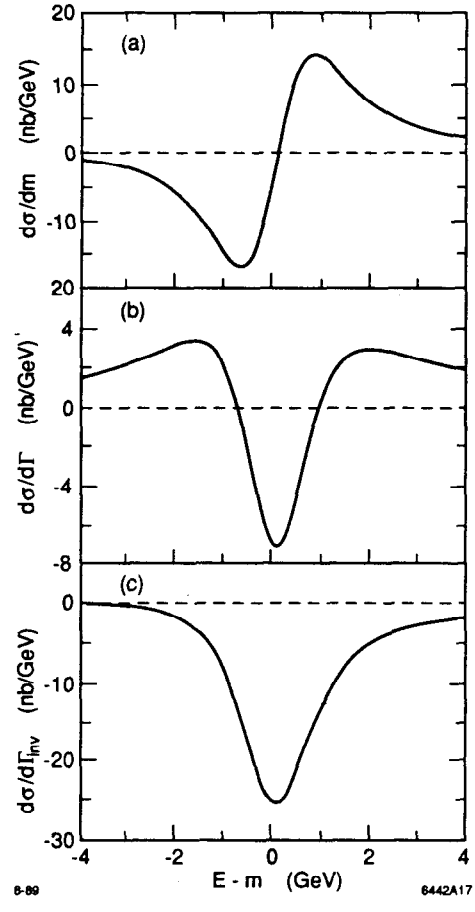

Figure 17. The derivatives of the Breit–Wigner shape, Eq. (4), with respect to the three fit parameters: (a) $d\sigma/dm$, (b) $d\sigma/d\Gamma$, and (c) $d\sigma/d\Gamma_{inv}$.

duce a Z and that it subsequently decays with unit probability. What we do not detect, then, must be those decays into neutrino pairs.

The sensitivities of the fits for the various parameters can be seen from the derivatives of Eq. (4), which are displayed in Fig. 17. The derivative $d\sigma/dm$ is an odd function, while both $d\sigma/d\Gamma$ and $d\sigma/d\Gamma_{inv}$ are even functions. This means that the determination of the mass is independent of the determination of the widths for scans which are symmetric with respect to the peak position. The determinations of Γ and Γ_{inv} differ in that the former is independent of the normalization (its derivative is bipolar), while the latter is strongly dependent on the normalization (its derivative is unipolar).

We perform three fits which differ in their reliance on the Standard Model, and thus address different questions that one may wish to ask.

1. In the "Standard Model Fit," m is the only parameter that is varied. The widths are taken to have their Standard Model values corresponding to the decays into five quarks and three charged and neutral leptons.
2. In the "Free ν Fit," both m and Γ_{inv} are allowed to vary. The visible width is constrained to its Standard Model value. The rationale for this is twofold:
   (a) New particle production in the quark-lepton sector might be expected to show up first with the lightest of particles, which, from the three examples we have seen so far, are the neutrinos.
   (b) Visible new particle production would probably show up first in the observation of distinctive decays.
3. Finally, the "Unconstrained Fit" allows all three parameters to be varied.

These fits are displayed in Fig. 18 and the results of the fits are displayed in Table 4. The mass values from the three fits are almost identical because of the orthogonality of the mass to the widths, as we just discussed. We choose the value from the Free ν Fit simply because it has the largest error. (I am often asked why the error on mass from the fit which has the most free parameters is the smallest. The reason is simple. First, the additional width parameters do not affect the mass determination because of the orthogonality of the functions. Second, the only scale of energy is the width. Since the unconstrained width is less than the Standard Model width, the error on the mass is smaller by roughly the same proportion.) All of the systematic errors in the mass determination are small, but the two largest sources of systematic uncertainty, included in the quoted errors, are 50 MeV for the MiniSAM efficiency and 40 MeV for the absolute energy determination.

The total width Γ is only determined by the Unconstrained Fit. The value of $1.95^{+0.40}_{-0.30}$ GeV should be compared to the Standard Model value of 2.46 GeV.[11] Two comments are in order:

1. The errors on the width are large because a good measurement of the width requires substantial data at ± 2 GeV from the peak, as can be seen from Fig. 17(b). We did not take very much data that far from the peak because the rate was just too low with our luminosity.
2. Although the width appears to be 1.3σ low, this is not a particularly meaningful statement be-

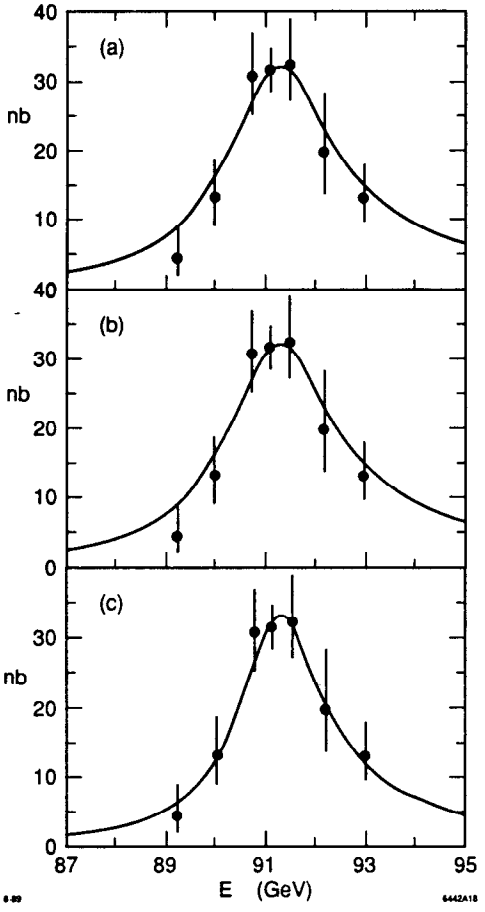

Figure 18. Fits to the cross section versus E. (a) the Standard Model Fit: m is free. (b) the Free ν Fit: m and Γ_{inv} are free. (c) the Unconstrained Fit: m, Γ, and Γ_{inv} are free.

Table 4: Results of the fits. The preferred values are shown in boldface. See text for explanation.

	Fit		
Variable (units)	Standard Model	Free ν	Unconstrained
m (GeV/c^2)	91.17 ±0.18	**91.17 ±0.18**	91.16 ±0.16
N_ν	-	**3.0 ± 0.9**	3.5 ± 0.8
Γ (GeV)	-	-	$\mathbf{1.95^{+0.40}_{-0.30}}$

cause the likelihood function, shown in Fig. 19, is not Gaussian. A Monte Carlo simulation shows that if the true width were the Standard Model value, 11% of experiments with our integrated luminosity and scanning strategy would get a value for the width equal to or less than the one we obtained.

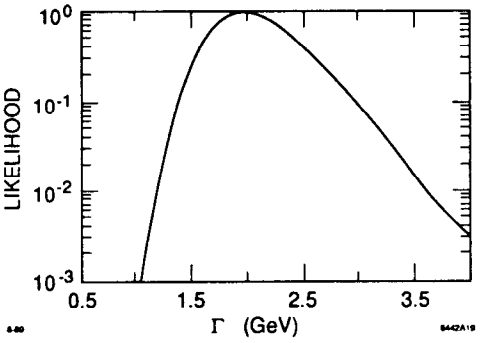

Figure 19. The relative likelihood function for Γ for the Unconstrained Fit.

Again all the systematic errors are small compared to the statistical error. The most significant contributions are 90 MeV from the uncertainty in the MiniSAM efficiency and 30 MeV from point-to-point energy uncertainties.

We take the value of $N_\nu = 3.0 \pm 0.9$ (or < 4.4 at the 95% confidence level) from the Free ν Fit as the preferred value. The value derived from the Unconstrained Fit cannot be interpreted as giving a consistent measurement of N_ν, since the fit has $\Gamma < \Gamma_{SM}$. This cannot happen in the Standard Model without a modification to the underlying gauge structure. However, in that case, Γ_{ee} and Γ_ν would not have Standard Model values, which we have assumed in calculating N_ν. The quoted errors include a contribution of 0.5 statistical and 0.25 systematic uncertainty coming from the overall absolute luminosity determination.

RELATIONSHIP BETWEEN THE MASS AND $\sin^2\theta_W$

The electroweak mixing angle, θ_W, can be expressed in terms of the Z mass by the relation

$$\sin 2\theta_W = \left(\frac{4\pi\alpha}{\sqrt{2} G_F m_Z^2 (1 - \Delta r)} \right)^{1/2} , \quad (5)$$

where Δr represents weak radiative corrections. These corrections arise from loops and are sensitive to the masses of high mass particles.

The most common definition of $\sin^2\theta_W$ is the Sirlin form,[12] which is defined as

$$\sin^2\theta_W \equiv 1 - \frac{m_W^2}{m_Z^2} . \quad (6)$$

For specific values of the two unknown masses in the Standard Model,

$$m_t = m_H = 100 \text{ GeV/c}^2 , \quad (7)$$

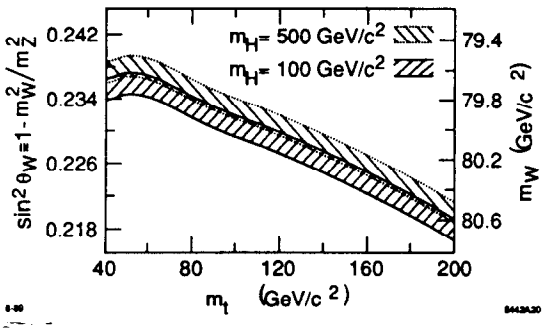

Figure 20. $\sin^2\theta_W$ as a function of the mass of the top quark for two values of the Higgs Boson mass. The bands represent ± 1 standard deviation about the values derived from Eq. (5).

our measured m_Z of 91.17 ± 0.18 GeV/c^2 implies

$$\sin^2\theta_W = 0.2307 \pm 0.0013 \ . \qquad (8)$$

The dependence of $\sin^2\theta_W$ on these two masses is shown in Fig. 20.

POSTSCRIPT

For the purpose of the historical record, the results given above were those reported at the Symposium. Between the time of the Symposium and the completion of this written version (mid-November 1989), the Mark II Collaboration doubled the data, from 233 events to 480 events, and published the following updated results[13]:

$$m = 91.14 \pm 0.12 \text{ GeV}/c^2 \ , \qquad (9)$$

$$\Gamma = 2.42^{+0.45}_{-0.35} \text{ GeV} \ , \quad \text{and} \qquad (10)$$

$$N_\nu = 2.8 \pm 0.6 \ . \qquad (11)$$

The last result translates into the upper limit

$$N_\nu < 3.9 \text{ at } 95\% \text{ C.L.} \ , \qquad (12)$$

which provides strong evidence that the number of light neutrino species is limited to the three that we have already discovered.

REFERENCES

1. The Mark II Collaboration consists of approximately 130 physicists from nine institutions: the California Institute of Technology, the University of California at Santa Cruz, the University of Colorado, the University of Hawaii, Indiana University, Johns Hopkins University, Lawrence Berkeley Laboratory, the University of Michigan, and the Stanford Linear Accelerator Center. The present members of the Collaboration are: G. S. Abrams, C. E. Adolphsen, R. Aleksan, J. P. Alexander, D. Averill, J. Ballam, B. C. Barish, T. Barklow, B. A. Barnett, J. Bartelt, S. Bethke, D. Blockus, W. de Boer, G. Bonvicini, A. Boyarski, B. Brabson, A. Breakstone, F. Bulos, P. R. Burchat, D. L. Burke, R. J. Cence, J. Chapman, M. Chmeissani, D. Cords, D. P. Coupal, P. Dauncey, H. C. DeStaebler, D. E. Dorfan, J. M. Dorfan, D. C. Drewer, R. Elia, G. J. Feldman, D. Fernandes, R. C. Field, W. T. Ford, C. Fordham, R. Frey, D. Fujino, K. K. Gan, C. Gatto, E. Gero, G. Gidal, T. Glanzman, G. Goldhaber, J. J. Gomez Cadenas, G. Gratta, G. Grindhammer, P. Grosse-Wiesmann, G. Hanson, R. Harr, B. Harral, F. A. Harris, C. M. Hawkes, K. Hayes, C. Hearty, C. A. Heusch, M. D. Hildreth, T. Himel, D. A. Hinshaw, S. J. Hong, D. Hutchinson, J. Hylen, W. R. Innes, R. G. Jacobsen, J. A. Jaros, C. K. Jung, J. A. Kadyk, J. Kent, M. King, S. R. Klein, D. S. Koetke, S. Komamiya, W. Koska, L. A. Kowalski, W. Kozanecki, J. F. Kral, M. Kuhlen, L. Labarga, A. J. Lankford, R. R. Larsen, F. Le Diberder, M. E. Levi, A. M. Litke, X. C. Lou, V. Lüth, G. R. Lynch, J. A. McKenna, J. A. J. Matthews, T. Mattison, B. D. Milliken, K. C. Moffeit, C. T. Munger, W. N. Murray, J. Nash, H. Ogren, K. F. O'Shaughnessy, S. I. Parker, C. Peck, M. L. Perl, F. Perrier, M. Petradza, R. Pitthan, F. C. Porter, P. Rankin, K. Riles, F. R. Rouse, D. R. Rust, H. F. W. Sadrozinski, M. W. Schaad, B. A. Schumm, A. Seiden, J. G. Smith, A. Snyder, E. Soderstrom, D. P. Stoker, R. Stroynowski, M. Swartz, R. Thun, G. H. Trilling, R. Van Kooten, P. Voruganti, S. R. Wagner, S. Watson, P. Weber, A. Weigend, A. J. Weinstein, A. J. Weir, E. Wicklund, M. Woods, G. Wormser, D. Y. Wu, M. Yurko, C. Zaccardelli, and C. von Zanthier.
2. G. S. Abrams *et al., Phys. Rev. Lett.* **63**, 724 (1989).
3. J. Kent *et al.*, SLAC–PUB–4922 (1989); M. Levi, J. Nash, and S. Watson, SLAC–PUB–4654 (1989); and M. Levi *et al.*, SLAC–PUB–4921 (1989).
4. G. S. Abrams *et al., Nucl. Instrum. Methods* **A281**, 55 (1984).
5. G. G. Hanson, *Nucl. Instrum. Methods* **A252**, 343 (1986).

6. G. S. Abrams *et al., IEEE Trans. Nucl. Sci.* **NS–25,** 309 (1978) and **NS–27,** 59 (1980).
7. F. A. Berends, R. Kleiss, and W. Hollik, *Nucl. Phys.* **B304**, 712 (1988); S. Jadach and B. F. L. Ward, University of Tennessee report UTHEP–88–11–01 (1988).
8. F. James and M. Roos, *Nucl. Phys.* **B172**, 475 (1980).
9. R. N. Cahn, *Phys. Rev.* **D36**, 2666 (1987), Eqs. (4.4) and (3.1).
10. J. Alexander *et al., Phys. Rev.* **D37**, 56 (1988).
11. Calculated using the program EXPOSTAR, assuming $m_t = m_H = 100\,\mathrm{GeV/c^2}$. D. C. Kennedy *et al., Nucl. Phys.* **B321**, 83 (1989).
12. A. Sirlin, *Phys. Rev.* **D22**, 2695 (1980).
13. G. S. Abrams *et al., Phys. Rev. Lett.* **63**, 2173 (1989).

DISCUSSION

R. Hofstadter, Stanford University: Do you need to include a correction for the Bhabha cross section because the e^+e^- scattering occurs in a high magnetic field?

G. Feldman: No, the magnetic fields from the SLC beams are far too weak to require such a correction.